JOURNAL OF SPACECRAFT AND ROCKETS
Vol. 47, No. 6, November–December 2010

Near-Infrared Spectroscopy of the Stardust Sample Return Capsule Entry: Detection of Carbon

Michael J. Taylor*
Utah State University, Logan, Utah 84322-4405
and
Peter Jenniskens†
SETI Institute, Mountain View, California 94043

DOI: 10.2514/1.38075

The 1069 nm line of atomic carbon was detected in radiation emitted during the 15 January 2006 reentry of the Stardust sample return capsule. In time-averaged data, the corresponding weaker lines in the range of 960–966 nm were also present. The spectra covered the wavelength range from 930 to 1075 nm at a spectral full-width-at-half-maximum resolution of 1.6 nm. The integrated 1069 nm line intensity decreased from 737 ± 44 $W/m^2/nm/sr$ at 80.7 km altitude (09:57:16.5 Universal Time) to 432 ± 44 $W/m^2/nm/sr$ at 70.9 km altitude (09:57:24.5 Universal Time). At the same time, the 1011 nm blend of nitrogen lines increased from 2110 ± 29 to 5378 ± 42 $W/m^2/nm/sr$. Absolute calibration errors add to these values a systematic uncertainty of about 20%. The capsule's heat shield consisted of a phenol-impregnated carbon ablator. Hence, the intensity of the carbon-atom line emission is a measure of the ablation rate during descent, but it also depends on the details of carbon-atom ablation and the excitation in the shock layer.

I. Introduction

THE manner in which carbon-based thermal protection materials ablate carbon is not yet fully understood. One such material, phenol-impregnated carbon ablator (PICA), was used in NASA's Stardust mission to protect a sample of comet 81P/Wild 2 during reentry. In arcjet tests of PICA ablation, Raiche and Driver [1] compared emission measurements from PICA tests with those of nonablating copper and Teflon targets. Carbon line emission was not detected. It was speculated that carbon was released in solid or molecular form rather than in atomic form. Indeed, continuum emission ahead of the shock was attributed to ejected solid material, likely carbon or carbon bearing, with a gray-body temperature that was close to that of the material surface [1].

The lack of detecting carbon-atom line emission could have been merely a lack of instrumental sensitivity and spectral resolution. Their spectral resolution was relatively low, and the strongest carbon lines transmitted by the atmosphere were outside the spectral range of the instrument. Alternatively, it is possible that the ablation conditions were not suitable for having high abundances of excited carbon atoms in the flow, for example, because the atoms would chemically react and form molecules and solid materials. That does not mean that carbon-atom line emission could not be detected in flight. It is seldom possible to simultaneously match all aspects of the flight environment in any ground test facility [2].

The return of Stardust on 15 January 2006 was the first test of PICA ablation in actual flight conditions [3]. The Stardust capsule entered Earth's atmosphere at a high relative velocity of 12.8 km/s (at 135 km altitude). An observing campaign was organized to study the ablation of PICA by remote sensing of emitted radiation during the hypervelocity entry of the Stardust capsule [4,5]. One objective of the observations was to detect carbon-atom line emission, to be used as a diagnostic tool for studying the specifics of ablation and excitation. The strongest carbon-atom emission lines transmitted by the atmosphere are at the near-infrared wavelengths of 910, 941, and 1069 nm (Fig. 1) [6]. At peak heating, the 1069 nm carbon line was expected to be about as strong as the nearby nitrogen lines at 1052 and 1055 nm [6]. In earlier meteor shower observations, the carbon-atom emission could not be resolved from these nearby nitrogen lines [7].

Here, we report on the successful detection of the 1069 nm line of carbon using a new instrument, designed to produce a higher spectral dispersion, which proved to be sufficient for detecting this line above the background continuum emission from the capsule's hot surface.

II. Instrument

A high-dispersive slitless near-IR spectrograph, called NIRSPEC (Fig. 2), was developed to be sensitive in the wavelength range from 930 to about 1100 nm, with a spectral resolution of full-width-at-half-maximum (FWHM) = 1.3 nm, able to resolve emission lines 2 nm apart.

The main sensor was a Sensors Unlimited, Inc. SU640SDV-1.7RT indium–gallium–arsenide (InGaAs) camera [8] with a 640 × 512 pixel (25 μm per pixel) detector array and a frame rate in excess of 29 frame/s. A Nikon 180/2.8 ED Nikkor automatic indexing lens was used with a 6.4 cm aperture. The diaphragm aperture was set at f2.8. The sensor was made of InGaAs, with a 53% proportion of InAs relative to GaAs, on an indium phosphide substrate. The camera had a 16 × 12 mm detector size and a field of view of 5.1 × 3.8° when equipped with a 180 mm focal length lens.

In front of the camera was placed an objective grism (shown schematically in Fig. 2), made for this experiment by Diffraction Products, Inc. The grism is a 78 × 85-mm-sized no. 3090 (600 groove/mm) transmission grating with a first-order blaze wavelength at 500 nm (28° 41' blaze angle), which is cemented to a BK7-glass right-angle prism with an apex angle of 30°. The grism was large enough to cover the full lens aperture. Grooves ran perpendicular to the line defining the maximum prism slope.

The camera was mounted on a trainable assembly built by M and O Precision Machine (Fig. 2). A co-aligned Xybion intensified camera was used for pointing. A second InGaAs camera with an extended sensitivity into the visual wavelength range, called VIS-NIR, was also on this assembly (Fig. 2).

Received 15 April 2008; revision received 5 May 2010; accepted for publication 6 May 2010.

*Center for Atmospheric and Space Science, 4405 Old Main Hill; mike.taylor@usu.edu.

†Carl Sagan Center, 515 N. Whisman Road; Petrus.M.Jenniskens@nasa.gov. Member AIAA (Corresponding author).

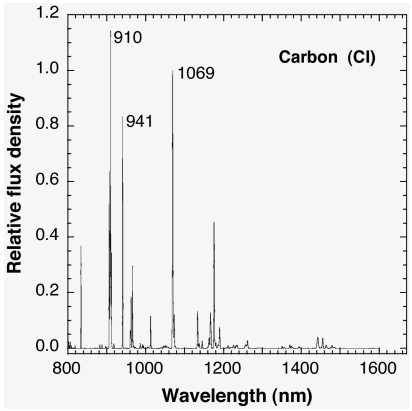

Fig. 1 Predicted carbon-atom line emission for an excitation temperature of 10,000 K [16].

The NIRSPEC camera was mounted at a small 6.5° angle from the boresight (Fig. 2) in such a way that, when the Xybion camera was pointed at the source, the central wavelength for the NIRSPEC was 991 nm and the wavelength range covered ranges from about 935 to 1075 nm. This interval covered both the anticipated 941, 960–966, and 1069 nm lines in Fig. 1 [6]. The exact wavelength coverage depended on the pointing direction of the camera and was slightly less later in flight, when the capsule moved more rapidly on the sky and the observer had some difficulty tracking the target.

The NIRSPEC camera was operated behind window port 1290 L, equipped with a flat Pyrex window (SN102) [9]. The transmission properties of the window were measured in the laboratory and found to be gray in the wavelength range discussed here.

The dynamic range of the camera was 14 bits, but the images were recorded at an 8-bit dynamic range (256 gray scales), at a frame rate of 29 Hz, on digital Hi-8 video (720 × 480 pixel). The Universal Time (UT) was imprinted directly on the video frames at a precision of ±0.001 s, and it was obtained from Global Positioning System-controlled interrange instrumentation group time code "B" (IRIG-B) provided in the aircraft. The time marker refers to the moment that the time code is written in the recorded data stream. Hence, the center of the exposure interval was expected to be 1/60 s earlier.

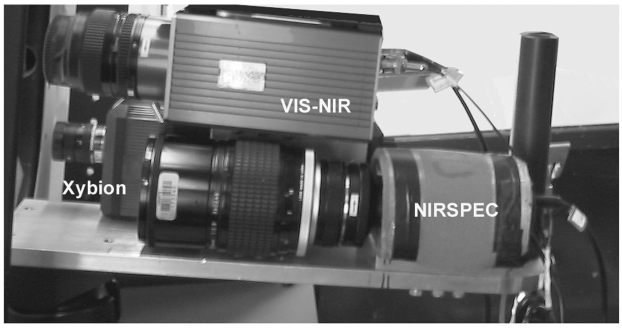

a)

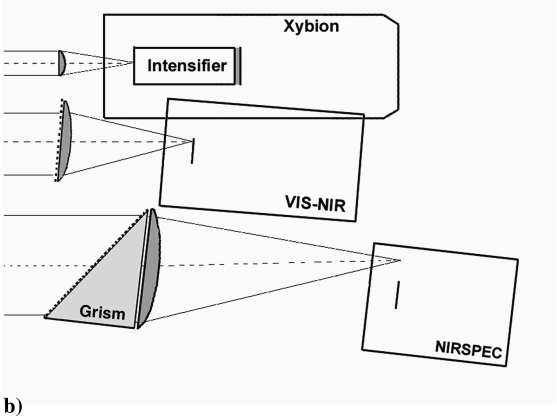

b)

Fig. 2 The three co-aligned cameras: NIRSPEC, VIS-NIR, and Xybion. a) This side view shows the camera assembly mounted in front of the window on a trainable assembly and NIRSPEC without the grism. b) Top view of the schematic layout of the instruments. Note that images are projected on the sensor in mirror orientation.

III. Observations

The Stardust sample return capsule (SRC) entry radiation was captured by the Xybion pointing camera as soon as rapid brightening occurred at around 09:57:05 UT (Fig. 3). The capsule was immediately tracked, initially moving very slowly in projection against the sky.

A total of about 1300 spectra were recorded. The continuum emission radiating from the hot surface of the capsule was first bright enough to record a spectrum at 09:57:12 UT. From the start, the spectrum was dominated by continuum emission (Fig. 4). At the same time, air plasma lines of nitrogen were detected, which increased in intensity until about 09:57:36 UT, after which the lines rapidly faded and only the continuum emission remained. The air plasma lines were last detected by NIRSPEC around 09:57:38 UT.

Tracking became difficult later in flight because the angular velocity of the capsule increased. After 09:57:25 UT, the pointing tended to lag the capsule's motion, and the spectrum shifted further out of the image frame, leaving a shorter range in wavelengths for study. No spectra were recorded around 09:57:36 and 09:57:50 UT, each time for only about 1 s.

The capsule was lost behind the window frame toward the end of the entry. Until 09:57:57, the grism surface was unobstructed by the lens of the VIS-NIR or Xybion cameras, but that was not the case after 09:57:57 UT. By that time, the viewing geometry had changed from a mostly frontal to a decidedly backward view of the capsule.

IV. Calibration

The spectra were oriented on the detector array at a small 1.5° angle relative to the pixel rows (Fig. 4). There was a nonzero background that required subtraction from the data images. Hence, each video frame was extracted, converted to grayscale, background-subtracted, and rotated by 1.5°, and a one-dimensional spectrum was extracted by adding the pixel brightness over a band of typically 9 pixel wide that covered the width of the spectrum. Those intensities were then corrected for instrumental response, while the pixel coordinate was translated to wavelength.

Fig. 3 The Stardust SRC entry as observed with the Xybion intensified camera.

Fig. 4 A typical spectrum of the Stardust SRC's entry radiation recorded by NIRSPEC at 09:57:26.720 UT. The capsule is to the left, outside the field of view. The wavelength scale runs from left to right and is defined by the nitrogen lines at 939 (left, start of spectrum) and 1011 nm (brightest dot).

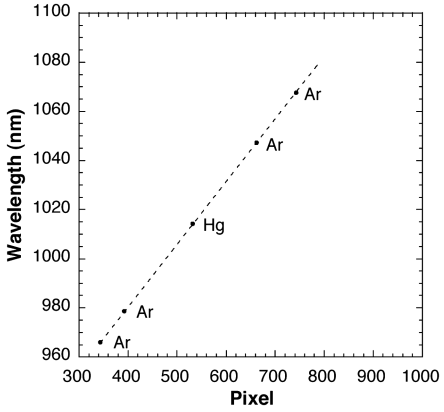

Fig. 5 Wavelength calibration from argon and mercury lines in the calibration lamp spectrum.

The instrumental dispersion was calibrated using an Ocean Optics HG-1 mercury argon line emission lamp (Fig. 5). Vacuum wavelengths were obtained from the Kurucz tables [10]. We identified the argon emission lines at 966.044, 978.719, 1047.292, and 1067.649 nm and the mercury line at 1014.2 nm [11]. The wavelength scale was linear in this part of the curve, with a dispersion of 0.2543 ± 0.0008 nm/pixel (in a 1.5° rotated frame). Based on this, we were able to identify the strongest atomic lines in the Stardust SRC spectra. We then did an internal wavelength calibration using the capsule's nitrogen line emissions (Table 1). This internal calibration guaranteed that the wavelength scale and dispersion pertained to a source at infinity and to the instrumental operation conditions during the observations.

The spectral resolution in terms of FWHM of the emission lines was, at best, 1.3 nm (5 pixel) over the range of the Stardust SRC entry observations (930–1080 nm). However, spatial movement of the target during each exposed frame in the dispersion direction from aircraft vibrations and irregularities of manual tracking (called motion blurring) tended to broaden the spectral lines, as did the imprecise alignment of noisy spectral lines, resulting in a more typical resolution of FWHM = 1.6 nm.

Spectra with significant motion blurring in the dispersion direction were not reduced. Fortunately, motion blurring was nearly absent early in flight, when the spectra were faint. Later, when the SRC moved faster across the sky and tracking became more difficult, the SRC was also much brighter, so that a single spectrum was often sufficient for good signal to noise. In the absence of emission lines, it was not possible to detect the presence of motion blurring from tracking errors after 09:57:38 UT.

The instrument's spectral sensitivity was calibrated over the full wavelength range of the instrument (Fig. 6) by observing a newly purchased Ocean Optics LS-1-CAL Tungsten calibration lamp (LSC1429), placed atop a line emission source, from a distance of several meters on the evening of January 13. The factory-provided lamp calibration curve was given from 300–1050 nm, but it needed to be corrected for fiber attenuation (a fiber being used in the Ocean Optics provided calibration) [12]. During the tarmac tests, the distance from lamp to the observer (about $D = 3.6 \pm 0.6$ m) was difficult to measure, because the instrument was mounted inside the aircraft, and the lamp was positioned on the tarmac. The calibrations were repeated in the laboratory on January 17, and again in April of 2006, using an Ocean Optics LS-1 tungsten lamp without the Teflon diffuser. This lamp was calibrated against a National Institute of Standards and Technology standard at the Stewart Radiance Lab. In the January 17 measurements, the distance was $D = 5.69$ m.

Measurements were made by pointing the camera first toward and then away from the source in steps of about half a frame. In this way, the spectrum was shifted in the field of view in small steps. While the spectral dispersion was too large to capture the full spectrum in the field of view, by pasting these individual scans together (after correcting for vignetting), a full spectrum was measured. We matched the individual scans of the spectrum as far as the identified argon and mercury lines would carry, then we anchored the remainder of the wavelength scale to the features in the 1.4 μm telluric water vapor absorption band. The shape of the water band was calculated using the moderate resolution atmospheric transmission (MODTRAN) program (air wavelengths). Each recorded image was corrected for vignetting and for geometric dilution of the incident light. The result was then divided by the flux density calculated from the calibration lamp curve and the solid angle of the exposed Teflon surface [12].

For the NIRSPEC measurements of the Stardust SRC reentry radiation, only the response in the wavelength range from 930 to 1080 nm is relevant. The 1.4 μm water vapor absorption band in Fig. 6 is a variable feature of the instrument response, as far as water vapor adsorbed on the window and in the line of sight from window to instrument is concerned. This absorption band will have been different when at altitude, but the strength of this band is of no concern, because it is fully outside the range of the Stardust SRC entry observations.

Table 1 Atomic emission lines identified in the Stardust SRC spectra

λ measured	λ theory	Atom
939.5	938.938	N
	939.537	N
	938.843	N
940.7	940.831	C
946.6	946.327	N
960.0	960.567	C
962.3	962.342	C
966.0	966.108	C
	982.544	N
986.6	986.604	N
	1000.578	N
1011.3	1010.790	N
	1011.166	N
	1011.525	N
	1011.741	N
1014.9	1013.106	N
	1015.005	N
	1016.763	N
1051.3	1050.988	N
	1051.629	N
	1052.346	N
1054.3	1053.665	N
	1054.246	N
	1055.253	N
	1056.622	N
1064.8	1064.690	N
1065.7	1065.596	N
	1067.687	N
1068.4	1068.601	C
1069.4	1069.417	C

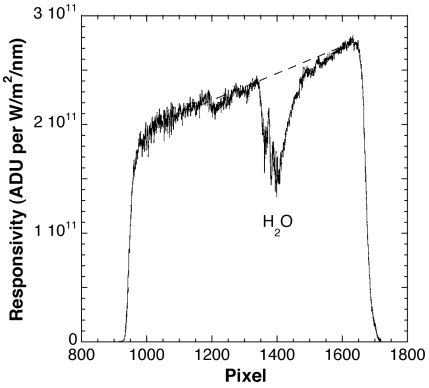

Fig. 6 Spectral responsivity of NIRSPEC, from tarmac calibrations (includes aircraft window transmission in near-perpendicular viewing).

Motion blurring perpendicular to the dispersion direction was caused deliberately after 09:57:25 UT, when the capsule became bright enough to saturate the spectra. While motion blurring spread out the light over more than 1 pixel, thus preventing saturation, some light may have been lost from the core of the recorded spectra. Because of that, it is necessary to align the continuum in each spectrum with that obtained from other experiments onboard the DC-8 during the observing campaign to obtain an absolute calibration. The effect of this will be addressed next.

V. Results

The result of extracted spectra for times 09:57:12.0 through 09:57:26.0 UT was averaged in 1 s intervals and compared with the less than 860 nm high-resolution spectra obtained by the echelle-based spectrograph for the crisp and high efficient detection of low light emission (ECHELLE) obtained between 09:57:16.0 and 09:57:26 UT [12]. The continuum level of the NIRSPEC data in this time frame was matched to the continuum measured by ECHELLE. The result is shown in Fig. 7.

A. Detection of Carbon Emission

Figure 7 shows the result in the wavelength range from 960 to 1080 nm. The strongest carbon emission in this wavelength range, the two lines at 1069 nm, are at the edge of the measured range. At the expected position is a strong line, which can be seen in individual images. The line is well resolved from nearby weak nitrogen lines at 1064.690, 1065.596, 1067.687, 1071.648, 1072.089, and 1073.345 nm. The line is also resolved from a potential weak oxygen line emission at 1067.88 nm. In our earlier meteor observations with a lower-resolution instrument, this separation was not achieved [7].

The average spectrum over the period from 09:57:12 to 09:57:25 UT is shown in Fig. 8. This spectrum also shows the weaker carbon-

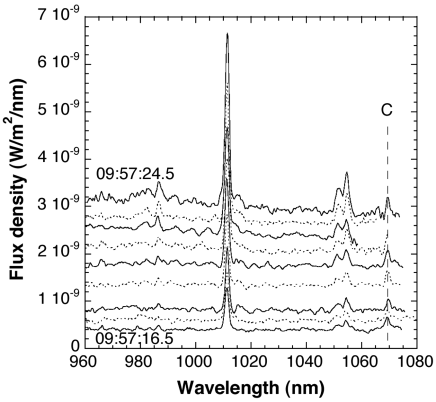

Fig. 7 Result for times 09:57:16–25 UT, in steps of 1 s. The carbon-atom line emission is marked.

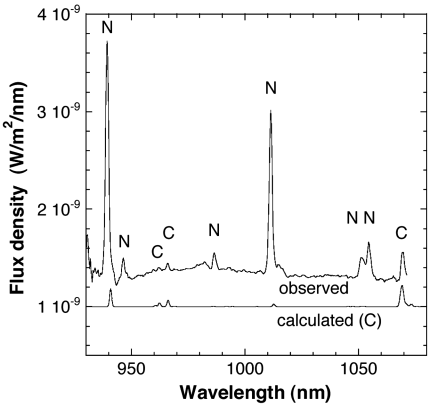

Fig. 8 Detection of carbon lines in 960–966 nm range. This is an average spectrum over the 09:57:12–09:57:25 UT interval. The theoretical emission of carbon is shown at the bottom of the figure (displaced for clarity).

atom lines at 960–966 nm. The underlying line in Fig. 8 shows the predicted carbon-atom flux for an excitation temperature of order 10,000 K. The intensity scale is scaled to match the observed 1069 nm carbon line brightness.

Other carbon-atom lines cannot be detected. The 941 nm line may be responsible for a shoulder on the stronger 939 nm nitrogen line. Because of the overlapping nitrogen line, however, we are not certain that this line has been detected. We did not detect the predicted emission at 991 nm in the publication by Jenniskens et al. [6]. Before reduction of the data, we had already discovered that the expected flux of the 991 nm line of carbon was incorrectly calculated and was too weak to plot in Fig. 8.

The strength of the 1069 nm line varied relative to that of the strong nitrogen lines at 1011, 1051, and 1054 nm. The lines were strongest relative to the nitrogen in our first recorded spectrum at 09:57:12 UT. At 09:57:16.5 UT, when the capsule had penetrated to 80.7 km altitude, the integrated 1069 nm line had an apparent flux of $2.19 \pm 0.13 \times 10^{-9}$ W/m^2/nm. With a projected surface area of 0.510 m^2 and a distance to the capsule of 416 km [12], this translates to an intensity of 737 ± 44 W/m^2/nm/sr.

Deeper down in the atmosphere, the carbon line became relatively weaker when compared with those of nitrogen. At 09:57:24.5 UT, when the capsule was at 70.9 km altitude, the apparent flux of the carbon emission was almost the same at $2.17 \pm 0.23 \times 10^{-9}$ W/m^2/nm, but the intensity had decreased to 432 ± 44 W/m^2/nm/sr (for a projected surface area of 0.506 m^2 and a distance to the capsule of 320 km [12]). At the same time, the nitrogen lines at 1011 nm increased in flux in an exponential manner from $2.70 \pm 0.03 \times 10^{-8}$ to $6.27 \pm 0.04 \times 10^{-9}$ W/m^2/nm and in intensity from 2110 ± 29 to 5378 ± 42 W/m^2/nm/sr. Systematic errors from the absolute calibration of flux add at least 20% to the uncertainty [12]. At the same time, other instruments show that the CN band intensity increased slightly between 81 and 71 km altitudes [12]. CN is thought to be a product of carbon atoms reacting with nitrogen molecules in the shock.

After 09:57:25 UT, including the period around peak heating at 09:57:33 UT, our spectra cut off just before the carbon line, which temporarily terminated the measurement. After 09:57:44 UT, the 1069 nm wavelength range came within view again. At that time, atomic lines of nitrogen and oxygen had decreased significantly. We checked to see if the carbon-atom line emission could be followed past the point where shock emissions ceased to be important. Other instruments still detected strong CN band emission at that time [13]. The carbon-atom lines, however, were not obvious in the individual spectra. Unfortunately, in the absence of air plasma emission lines, this made it hard to recognize the motion blurring of lines in the dispersion direction of the grating and made it impossible to align the spectra accurately to bring out the weaker emission lines by averaging spectra over a 1 s interval. The strong nitrogen and oxygen lines were used to align the spectra when averaging data in 1 s intervals.

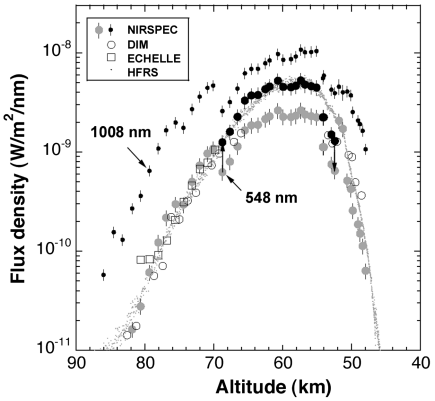

Fig. 9 Comparison of NIRSPEC flux (corrected for extinction) measured at 1008 nm and extrapolated to the 548 nm flux. Results are compared with those derived from other instruments [12,14,15]. The different data sets are explained in the text.

B. Continuum Emission

As a control on the sensitivity calibration, we compared the measured near-IR flux to that expected from the continuum flux measured by other instruments in the observing campaign. The observations provided a record of continuum emission in the wavelength range from 960–1050 nm.

Figure 9 shows the observed continuum flux at ∼1008 nm (mean of 1003 and 1013 nm flux) as a function of altitude of the capsule (•). A small correction is applied to remove telluric extinction (factor 0.96–0.99).

From the flux at 1008 nm, the flux at 548 nm was calculated (gray dot) assuming that the continuum emission had the wavelength dependence of a blackbody with the altitude-dependent mean surface temperature profile derived in Trumble et al. [13].

This result is compared with that derived with other instruments deployed during the observing campaign, in particular, to that derived from the ECHELLE [12] spectrograph (open squares), from the digital imager (DIM) [14] (○), and from the high frame-rate spectrograph (HFRS) [15] instrument (small dots).

In general, there is good agreement down to 70 km altitude. Below that, the NIRSPEC flux suddenly falls a factor of two below that measured by HFRS. The NIRSPEC camera seems to recover after peak heating, when the apparent flux density has fallen back to below $\sim 2 \times 10^{-9}$ W/m^2/nm (Fig. 9). We suspect that an automatic gain change is responsible for this drop in sensitivity.

At times, the integrated flux dropped below that expected for a full 1 s exposure. It is possible that tracking errors may have caused some flux to be lost in motion blurring at times when motion blurring was introduced deliberately to avoid saturation.

VI. Conclusions

Ablation of PICA does produce carbon atoms during actual reentry conditions. The carbon-atom line at 1069 nm was detected periodically between 09:57:12 and 09:57:25 UT, when the relevant wavelength range was in view. The line strength was measured to an accuracy of about 20%, when averaged over a 1 s time interval. During this time interval, the apparent carbon-atom line flux density measured at the aircraft was nearly constant, unlike the nitrogen and oxygen line emissions from the shock wave, which increased exponentially with time.

The 1069 nm line was proven strong enough to be detected above the continuum radiation from the hot capsule's surface, which makes this atomic line a suitable diagnostic in laboratory measurements of PICA ablation. It remains to be seen, however, whether laboratory conditions can reproduce the actual flight conditions during descent of the Stardust capsule between 81 and 71 km, where carbon-atom line emission was detected. While the ablation rate was expected to increase moving toward peak heating, the carbon-atom line intensity decreased.

These data may be used to better understand the relationship between carbon ablation and the radiation of carbon atoms in the emitting gas, an important problem in meteor astronomy [16]. Carbonaceous compounds ablated in meteors are a potential source of prebiotic molecules needed for the origin of life on Earth but, so far, carbon-atom line emission has not been conclusively detected in meteors [7].

In future applications, the camera could be oriented at a slightly higher angle to keep this spectral range in view even when tracking becomes difficult. The Stardust reentry data are available now for interpretation. The observations of the Stardust SRC entry are expected to remain a unique system field test for a long time to come. The observational data and the calibration files will be archived for this purpose. The present paper serves to document the files in hand.

Acknowledgments

This work was funded and managed by the Orion Thermal Protection System Advanced Development Project and the NASA Engineering and Safety Center. We thank Mitsumu Ejiri for helping operate the camera. E. Leibhardt of Diffraction Products, Inc. made the grism. Tara Martin of Sensors Unlimited, Inc. made this camera available for us to use. Dominique Pautet assisted in the data reduction. Calculations of expected emission levels by Mike Wright and Joe Olejniczak at NASA Ames Research Center made it possible for us to set the instrument settings correctly. We thank Stephen Burress of Oceon Optics for helpful insight. Dave E. Jordan of NASA Ames Research Center acted as the NASA program manager for the mission and designed methods for instrument installation. Jeff Ignaitis from M and O Precision Machining designed and built the instrument's mounting hardware. NASA's DC-8 Airborne Laboratory was deployed by the University of North Dakota/ National Suborbital Education and Research Center, under contract with NASA Wallops Flight Center.

References

[1] Raiche, G. A., and Driver, D. M., "Shock Layer Optical Attenuation and Emission Spectroscopy Measurements During Arc Jet Testing with Ablating Models," 42nd AIAA Aerospace Sciences Meeting and Exhibit, AIAA Paper 2004-825, Jan. 2004, 2004.

[2] Wright, M. J., Grinstead, J. H., and Bose, D., "A Risk-Based Approach for Aerothermal/TPS Analysis and Testing," AVT-142 RTO AVT/VKI Lecture Series, Feb. 2006, NATO Research and Technology Organization, 2007.

[3] Kontinos, D. A., and Stackpoole, M., "Post-Flight Analysis of the Stardust Sample Return Capsule Earth Entry," 46th AIAA Aerospace Sciences Meeting and Exhibit, AIAA Paper 2008-1197, Jan. 2008, 2008.

[4] Jenniskens, P., Kontinos, D., Jordan, D., Wright, M., Olejniczak, J., Raiche, G., Wercinski, P., Desai, P. N., Taylor, M. J., Stenbaek-Nielsen, H. C., McHarg, M. G., Abe, S., Rairden, R. I., Albers, J., Winter, M., Harms, F., Wolf, J., ReVelle, D. O., Gural, P., Dantowitz, R., Rietmeijer, F., Hladiuk, D., and Hildebrand, A. R., "Preparing for the Meteoric Return of Stardust," *Proceedings of Dust in Planetary Systems*, edited by A. Grapps, and E. Gruen, ESA SP 643, Paris, Sept. 2005, pp. 7–10.

[5] Kontinos, D. A., Jordan, D. J., and Jenniskens, P., "Stardust Airborne Observation Campaign Support," NASA Engineering and Safety Center Report RP-06-80, Aug, 2006.

[6] Jenniskens, P., Wercinski, P., Olejniczak, J., Raiche, G., Kontinos, D., Allen, G., Desai, P. N., ReVelle, D., Hatton, J., Baker, R. L., Russell, R. W., Taylor, M., and Rietmeijer, F., "Preparing for Hyperseed MAC: An Observing Campaign to Monitor the Entry of the Genesis Sample Return Capsule," *Earth, Moon, and Planets*, Vol. 95, Nos. 1–4, 2004, pp. 339–360. doi:10.1007/s11038-005-9021-2

[7] Taylor, M. J., Jenniskens, P., Nielsen, K., and Pautet, D., "First 0.96–1.46 Micron Near-IR Spectra of Meteors," *Advances in Space Research*, Vol. 39, No. 4, 2007, pp. 544–549. doi:10.1016/j.asr.2006.05.017

[8] Sensors Unlimited, Inc., "SU640SDV-1.7RT, SU640SDV-1.7RT-15 Hz High Resolution InGaAs SWIR Area Camera," Brochure No. 4110-0075, Rev. 2, April 2005.

[9] "DC-8 Experimenters Hand Book," NASA Dryden Flight Research

Center, Electronic publication, 2003, www.espo.nasa.gov/docs/intex-na/DC8_Handbook-1.pdf [retrieved 23 Dec. 2005].

[10] Kurucz, R. L., and Bell, B., Kurucz 1995 Atomic Line Data [CD-ROM], No. 23, Smithsonian Astrophysical Obs., Cambridge, MA, 1995.

[11] Hinkle, K. H., Joyce, R. R., Hedden, A., and Wallace, L., "Wavelength Calibration of Near-Infrared Spectra," *Publications of the Astronomical Society of the Pacific*, Vol. 113, No. 783, 2001, pp. 548–566. doi:10.1086/320280

[12] Jenniskens, P., "Observations of the Stardust Sample Return Capsule Entry with a Slit-Less Echelle Spectrograph," *Journal of Spacecraft and Rockets*, Vol. , No. , 2010, pp. (to be published).

[13] Trumble, K. A., Cozmuta, I., Sepka, S., Jenniskens, P., and Winter, M., "Postflight Aerothermal Analysis of the Stardust Sample Return Capsule," *Journal of Spacecraft and Rockets*, Vol. 47, No. 5, 2010, pp. 765–774. doi:10.2514/1.41514

[14] Jenniskens, P., and Wercinski, P., "Digital Still Snapshots of the Stardust Sample Return Capsule Entry," *Journal of Spacecraft and Rockets*, Vol. , No. , 2010, pp. (to be published).

[15] McHarg, M. G., Stenbeak-Nielsen, H. C., Kanmae, T., and Jenniskens, P., "Observations of the Stardust Sample Return Capsule Using a High Frame Rate Slit-Less Spectrograph," *Journal of Spacecraft and Rockets*, Vol. , No. , 2010, pp. (to be published).

[16] Jenniskens, P., "Quantitative Meteor Spectroscopy: Elemental Abundances," *Advances in Space Research*, Vol. 39, No. 4, 2007, pp. 491–512. doi:10.1016/j.asr.2007.03.040

D. Kontinos
Guest Editor